Supplementary Information

Mechanism of Li_2S formation and dissolution in Lithium-Sulphur batteries

Christian Prehal[1, *], Sara Drvarič Talian[2], Alen Vizintin[2], Heinz Amenitsch[4], Robert Dominko[2, 3], Stefan A. Freunberger[5, *], Vanessa Wood[1, *]

1. Department of Information Technology and Electrical Engineering, ETH Zürich, Gloriastrasse 35, 8092 Zürich, Switzerland
2. Department of Materials Chemistry, National Institute of Chemistry, Hajdrihova 19, 1000 Ljubljana, Slovenia
3. Faculty of Chemistry and Chemical Technology University of Ljubljana, Večna pot 113, 1000 Ljubljana, Slovenia
4. Institute for Inorganic Chemistry, Graz University of Technology, Stremayrgasse 9, 8010 Graz, Austria
5. IST Austria (Institute of Science and Technology Austria), Am Campus 1, 3400 Klosterneuburg, Austria

* Corresponding authors' e-mail: cprehal@ethz.ch, stefan.freunberger@ist.ac.at, vwood@ethz.ch

Supplementary Figures

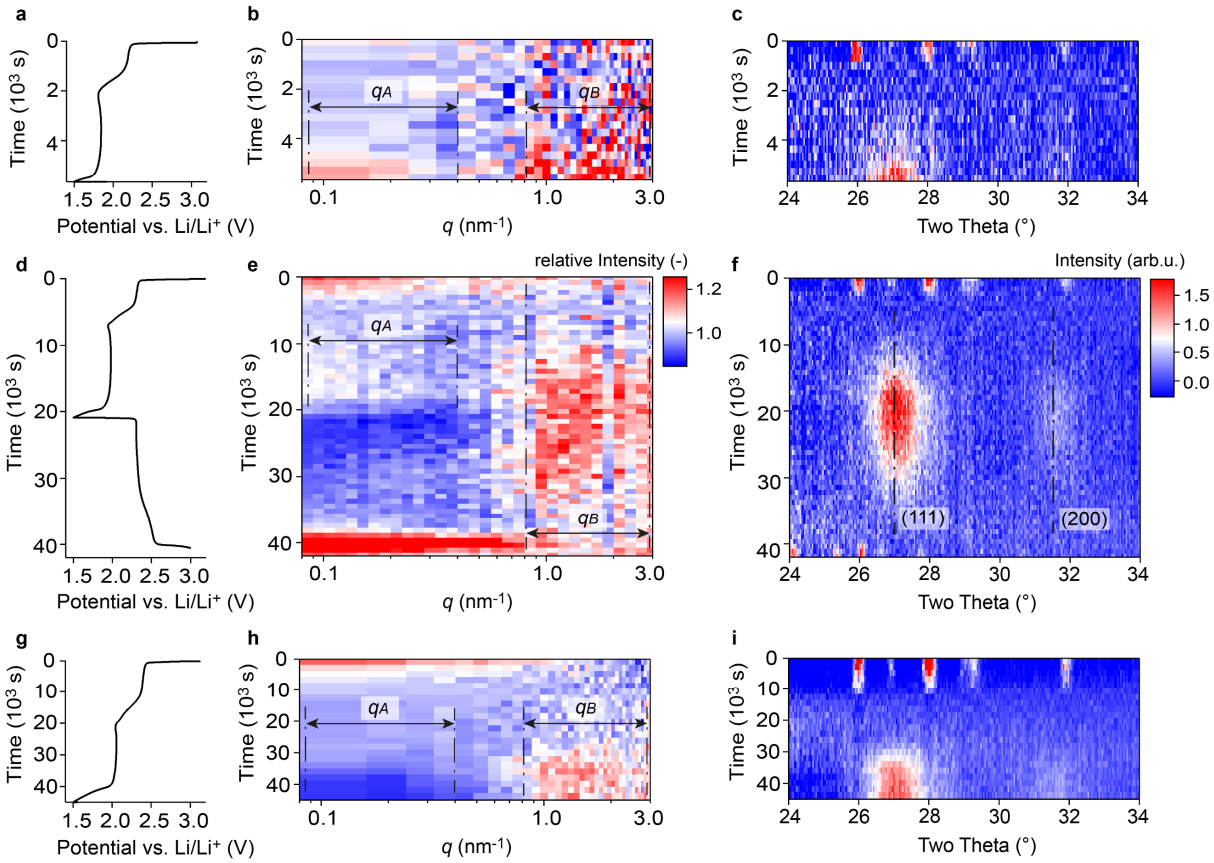

Supplementary Figure 1: In situ SAXS / WAXS during galvanostatic discharge / charge of a ENSACO350G/S composite cathode and a 1 M LiTFSI TEGDME:DOL (1:1) electrolyte at C/3 (**a-c**), C/10 (**d-f**) and C/30 (**g-i**). The SAXS/WAXS data were recorded on a laboratory SAXS facility (SAXSpoint 2.0, Anton Paar), resulting in a significantly higher signal-to-noise ratio as compared to the Synchrotron data. **a**, Potential vs. Li/Li+ as a function of time during galvanostatic discharge at C/3. **b**, The corresponding relative SAXS intensity change as a function of time and scattering vector length q. **c**, WAXS intensity as a function of time and scattering angle Two Theta. d-e and h-i show the same data for a full galvanostatic discharge / charge cycle at C/10 (**d-e**) and galvanostatic discharge at C/30 (**h-i**). The SAXS/WAXS data verify the important features observed in Fig. 2 in an alternative Li-S systems. The high-q (qB) SAXS intensity maximum at the end of discharge is present at all rates; the low-q (*qA*) SAXS intensity maximum is more pronounced at higher C-rates. The Scherrer crystallite sizes at C/3, C10 and C/30 correspond to 6.5 nm, 6.7 nm and 6.0 nm obtained from a Lorentzian peak fit and the Scherrer equation. This is practically identical to the values shown in Fig. 2. The sharp peaks in **c, f, i** correspond to the diffraction peaks of the relatively large sulfur crystallites.

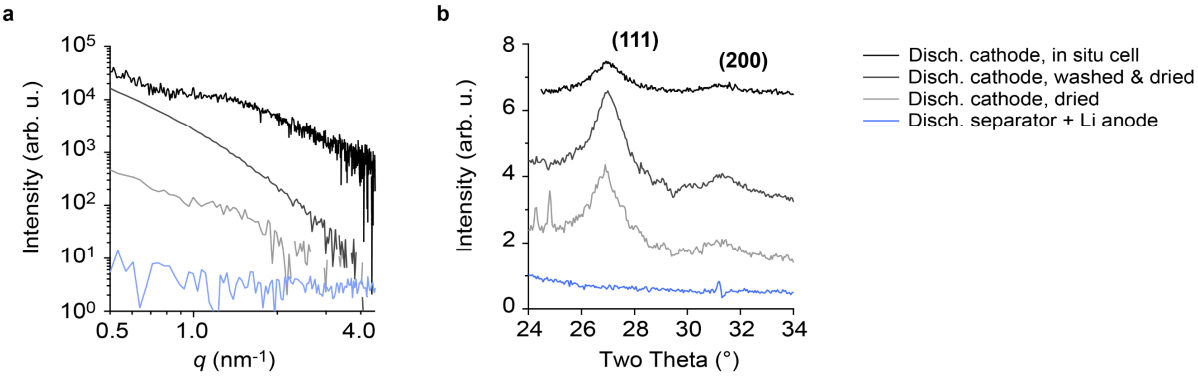

Supplementary Figure 2: SAXS/WAXS intensities versus scattering vector length *q* (**a**) and scattering angle (**b**) for the discharged cathode in the *in situ* cell. The black solid line shows the equivalent to the reduced SAXS intensity after discharge in Fig. 5a, the discharged cathode after washing with glyme and subsequent drying under vacuum (dark grey solid line) and the discharged cathode without washing, but with drying under vacuum (grey solid line). The blue solid line shows the SAXS/WAXS intensities of separator and Li metal after discharger. The absence of any SAXS feature and the Li_2S diffraction peaks gives evidence that the recorded structural changes take place in the cathode only.

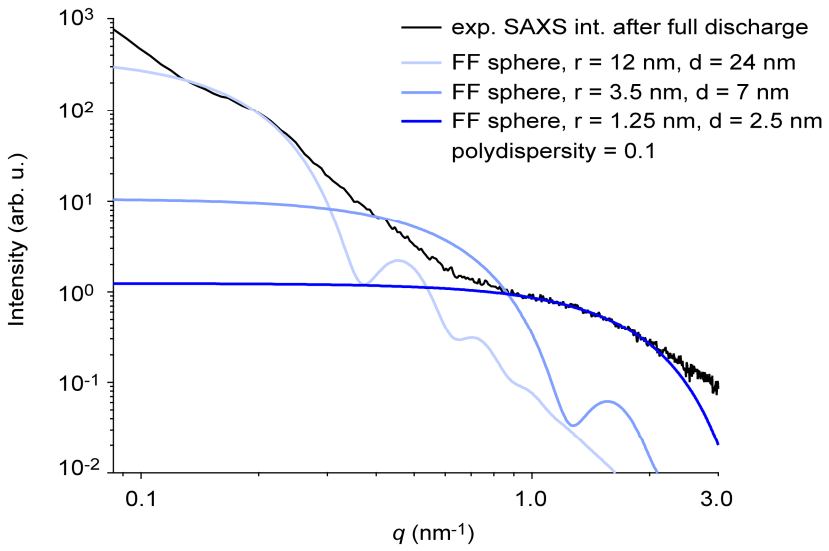

Supplementary Figure 3: Reduced, experimental SAXS intensity versus scattering vector length q for the fully discharged KB cathode in the diglyme catholyte after subtracting the SAXS intensity prior to discharge at OCV and hence the carbon black scattering contribution (black solid line, details see methods, all SAXS intensities during discharge are shown in Fig. 5a). The blue curves correspond to the analytical SAXS formfactor of spheres with 10 % polydispersity and a mean diameter of 24 nm, 7 nm and 2.5 nm and give an estimate about the size of possible real-space structures. The primary Li_2S crystallites with a size of 7 nm (as obtained from the Li_2S WAXS diffraction peak width) are not present as individual, solid particles since the corresponding intensity shoulder is missing in the SAXS regime. The high-q (1.5 nm^{-1}) and low-q (0.2 nm^{-1}) intensity shoulders correspond to solid particles / aggregates with a size around 2.5 nm and 24 nm, respectively.

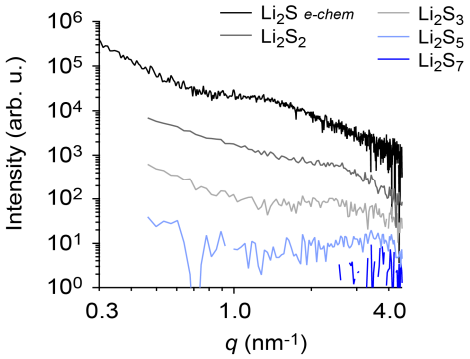

Supplementary Figure 4: SAXS intensity versus scattering vector length q of nominal Li_2S_2, Li_2S_3, Li_2S_5, Li_2S_7 polysulfide powders. The black solid line shows the SAXS intensity of the reduced in situ SAXS intensity at the end of discharge (equivalent to Fig. 5a). The corresponding XRD data is given in Fig. 4b. Li_2S_2 and Li_2S_3 show an intensity shoulder at high q, similar like the electrochemically formed Li_2S/Li_2S_4 deposits shown in Fig. 5. The presence of the intensity shoulder at higher q-values may point at smaller Li_2S_4 particles also present in the polysulfide powders.

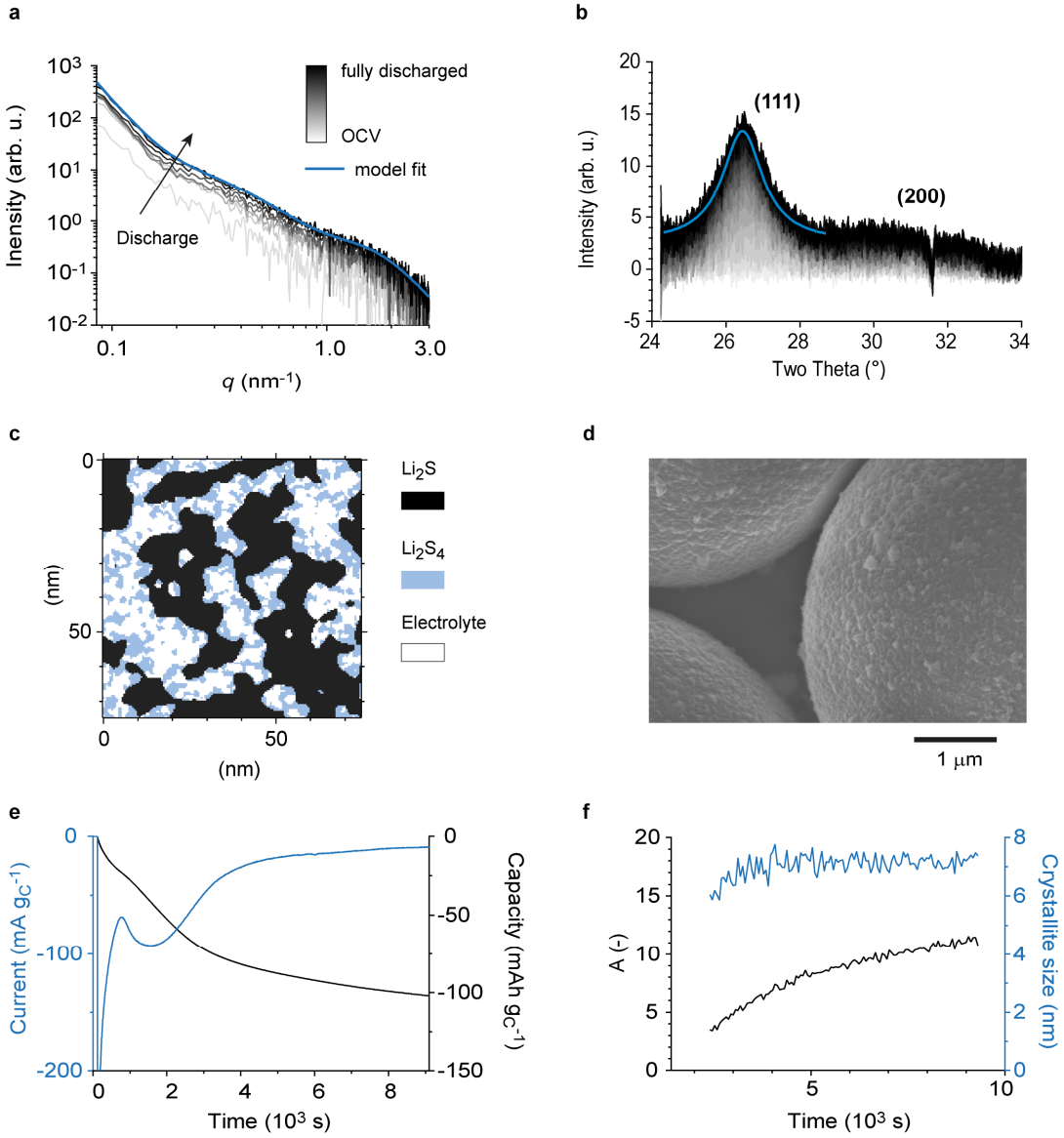

Supplementary Figure 5: In situ SAXS / WAXS and plurigaussian random field model for potentiostatic discharge with a Glassy Carbon bead cathode and the 0.5 M Li_2S_8 / 2G catholyte as used in Fig. 1, 2, 3, 5. **a**, reduced SAXS intensities versus scattering vector length *q* during potentiostatic discharge at 2.0 V vs. Li/Li⁺ to a capacity of 102 mAh g_C^{-1}. The SAXS intensity prior to discharge (at OCV) was subtracted from averaged SAXS intensities. The plurigaussian random field (PGRF) model fit is given in blue. Fit parameters are given in Table S1. **b**, Background corrected WAXS intensities versus scattering angle during potentiostatic discharge at 2.0 V vs. Li/Li⁺ to a capacity of 250 mAh g_C^{-1}. The (111) Li_2S diffraction peak is fitted using a Lorentz function. **c**, Cross section of the representative real space model generated via PGRFs and the input parameters obtained from the model fit in **a**. **d**, Scanning electron microscopy image showing the Li_2S deposits on top of the large Glassy carbon beads (> 1 µm) after potentiostatic discharge. **e**, Specific current (blue) and specific capacity (black) versus time during potentiostatic discharge of the in situ SAXS cell. Both current and capacity are normalized by the bare glassy carbon electrode mass. **f**, (111) diffraction peak height *A* (obtained from Lorentzian peak fit) and crystallite size (obtained from the (111) peak width and the Scherrer equation) as a function of time during potentiostatic discharge. The good fit quality in **a** indicates that the deviation in Fig. 5a stem from neglected Li_2S / Li_2S_4 – carbon black correlations. As the glassy carbon beads are much larger than the Li_2S / Li_2S_4 deposits any cross correlations are negligible in the SAXS intensities.

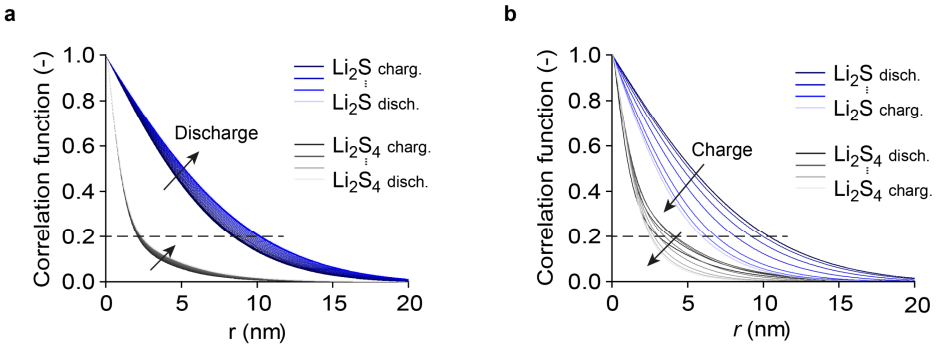

Supplementary Figure 6: a-b, Li_2S – Li_2S (blue to light grey) and Li_2S_4 – Li_2S_4 (black to light grey) correlation functions versus distance *r* of the Plurigaussian random field model in Fig. 5e-h, during discharge (**a**) and charge (**b**). The normalized correlation functions are calculated from the two-point probability functions as described in the methods section. The Li_2S and Li_2S_4 correlation length (shown in Fig. 5g, h) is (arbitrarily) defined as the distance *r*, where the correlation function reaches the value of 0.2.

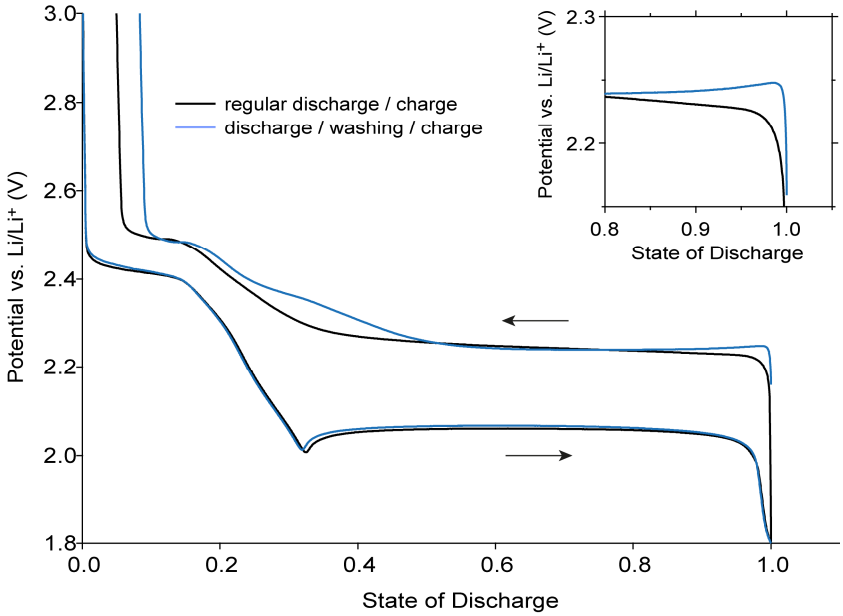

Supplementary Figure 7: Galvanostatic discharge / charge of a sulfur melt-infiltrated KB cathode (S:C mass ratio of 2:1) in 1 M LiTFSI + 0.4 M $LiNO_3$ / 2G at C/10 with a maximum discharge capacity of 1117 mAh g_S^{-1} (black curve) and 1231 mAh g_S^{-1} (blue curve). The black solid line shows a regular discharge / charge cycle. The blue solid line shows an identical galvanostatic discharge / charge cycle with an additional washing step of the discharged cathode between discharge and charge. The washing step includes rinsing the discharged cathode with 2G solvent, drying the washed and discharged cathode under vacuum, and reassembling the cell using the washed cathode, a new separator and a fresh 1 M LiTFSI + 0.4 M $LiNO_3$ / 2G electrolyte. The overpotential at the onset of charge shows that washing removes parts of the dissolved Li_2S_2 polysulfides and solid Li_2S_4 particles. Without the dissolved PSs serving as mediators initial charging requires the direct oxidation of Li_2S and hence electron transport across the poorly conducting Li_2S. In line with the first charging cycle of Li-S batteries using Li_2S / C composite cathodes[1], charging overpotentials in the beginning are high. The charging overpotential drops to values of the regularly cycled cell (black solid line) after a significant amount of dissolved PSs have been formed.

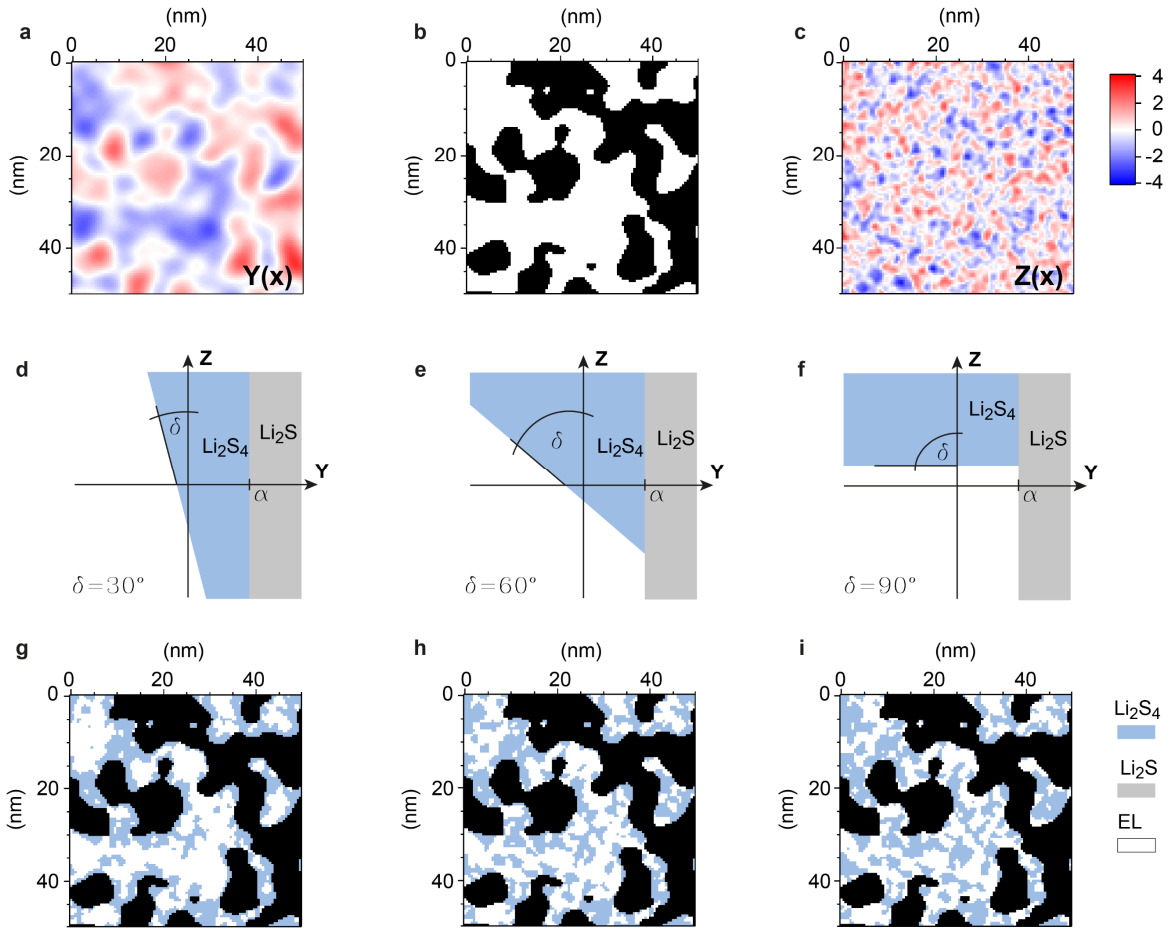

Supplementary Figure 8: Plurigaussian random field (PGRF), real space structure generation with the parameters shown in Table S1, second column. Only the parameter δ is varied. **a**, Cross-section of 3D Gaussian random field $Y(\boldsymbol{x})$. **b**, Cross section of 3D Li_2S structure generated from $Y(\boldsymbol{x})$ using the threshold value α. **c**, Cross-section of 3D Gaussian random field $Z(\boldsymbol{x})$. **d-e**, Z-Y planes visualizing the threshold value dependencies of the two GRFs $Y(\boldsymbol{x})$ and $Z(\boldsymbol{x})$. The threshold value α to generate the Li_2S structure is indicated on the horizontal axis. The borderline between blue and white area determines whether the Li_2S_4 phase shows a strong correlation (**d**, $\delta \to 0°$) or no correlation (**f**, $\delta \to 90°$) to the Li_2S phase. The corresponding morphologies for $\delta = 30°$, $\delta = 60°$, and $\delta = 90°$ are shown in **g**, **h** and **i**, respectively.

Supplementary Tables

Table S1 | **PGRF model fit results.** ρ_{e^-} is given in units of cm^{-2} and corresponds to the electron density times the classical electron radius (2.82×10^{-13} cm).

	Carbon black electrode (Model fit Fig. 5a)	Glass Carbon electrode (Model fit Supplementary Fig. 5a)
K	10	5.5
V / V_{max}	1	1
$\rho_{e^-, EL}$ (cm^{-2})	1.10×10^{11}	1.10×10^{11}
$\rho_{e^-, Li2S}$ (cm^{-2})	1.34×10^{11}	1.34×10^{11}
$\rho_{e^-, Li2S4}$ (cm^{-2})	1.52×10^{11}	1.52×10^{11}
l_Y (nm)	0.9	1.1
d_Y (nm)	6.0	4.6
l_Z (nm)	7.0	3.2
d_Z (nm)	48	32
ϕ_{Li2S}	0.4	0.48
ϕ_{Li2S4}	0.2	0.24
δ (°)	45	45
A	0.03	0.007
γ	–4	–4.5

Table S2 | **Electron (scattering length) densities of the various components.** ρ_{e^-} is given in units of cm^{-2} and corresponds to the electron density times the classical electron radius (2.82×10^{-13} cm). The Li_2S_4 mass density, 1.82 cm^3 g^{-1}, was taken from DFT simulations, calculating crystal structures of solid PSs[2]. For the catholyte, we assumed a Li_2S_8 concentration of 2 M inside the carbon black pores, i.e., higher than in the bulk liquid (0.5 M). The electron (scattering length) density of the as-prepared catholyte with 0.5 M Li_2S_8 corresponds to 0.98×10^{11} cm^{-2}. The carbon black skeleton density is lower than the graphite density due to the significant micropore content[3,4].

	Mass density (g cm^{-3})	Molar mass (g mol^{-1})	Molar volume (cm^3 mol^{-1})	ρ_{e^-} (cm^{-2})
Li_2S	1.66	45.95	27.68	1.34×10^{11}
Li_2S_4	1.82	142	73.57	1.52×10^{11}
S	2.00	32	16	1.69×10^{11}
Catholyte	-	-	-	0.98×10^{11}
Carbon	2.05	12	5.85	1.74×10^{11}

Supplementary Notes

Supplementary Note 1 | Discussion of alternative SAXS data interpretation

The SAXS model presented in Fig. 5 is consistent with all electrochemical (Fig. 1b), *in situ* SAXS (Fig. 2), *in situ* WAXS (Fig. 2), SEM (Fig. 3) and *ex situ* SAXS/WAXS data (Fig. 4b, Supplementary Figs. 2, 4). Focusing on the SAXS/WAXS data, we argue in the following why alternative interpretations remain possible, yet unlikely.

Why is the high-*q* intensity shoulder (Fig. 5a) likely caused by Li_2S_4 (or similar higher-order PS)?

An alternative interpretation of the high-*q* intensity shoulder in Fig. 5a could be a second fraction of smaller Li_2S particles generated by a mechanism other than disproportionation. While a large fraction of Li_2S would still be formed via solution-mediated disproportionation (as confirmed by the *in situ* WAXS data), a certain amount of Li_2S could be formed via direct electroreduction at the carbon-electrolyte interface. However, this is unlikely, as a conformal or somewhat patchy coating of Li_2S on the carbon black surface would decrease the high-*q* SAXS intensity[5].

As shown in Supplementary Fig. 9b, the structure causing the high-*q* intensity shoulder requires a higher electron density than its surrounding. Otherwise the significant intensity hump could not be reproduced.

A change in the electrolyte's electron density causes a larger scattering intensity change at low *q* (Supplementary Fig. 9a). This reflects the high sensitivity of the Li_2S aggregate structures against electrolyte electron density changes, due to the low Li_2S electron density (Supplementary Fig. 9a). This is best seen in the experimental SAXS intensity change directly after charging has started (Supplementary Fig. 9b). The quick increase in anion concentration causes a quick increase in the electrolyte electron density and hence a quick SAXS intensity drop (due to the reduced Li_2S–electrolyte electron density contrast $\Delta\rho_{Li_2S-El}$), specifically at low *q*. If the same material would cause both the low-*q* and high-*q* intensity shoulders, the intensity drop would be the same for all *q*.

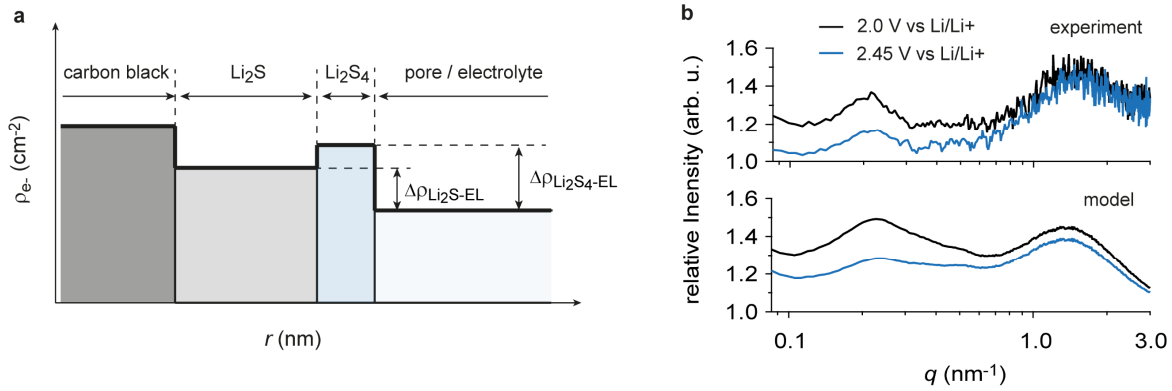

Supplementary Figure 9: a, Sketch of electron density levels ρ_{e^-} of the different phases. ρ_{e^-} is given in units of cm^{-2} and corresponds to the electron density times the classical electron radius (2.82×10^{-13} cm). The electron density contrast with respect to the surrounding phase determines the phase's "scattering power". **b**, relative SAXS intensities as a function of scattering vector length *q* at the end of discharge at 2.0 V vs. Li/Li^+ (black) and right after charge has started at 2.45 V vs. Li/Li^+ (blue) for the experimental data (top) and the PluriGRF SAXS model (bottom). To obtain the relative SAXS intensities, the SAXS intensities were normalized by the SAXS intensity prior to discharge at OCV. The difference in the relative SAXS intensities in **b** is primarily caused by the quick change in the electrolyte electron density. The relative SAXS intensity change for both model and experimental data is larger at small q and smaller at high *q* – indicating that the high-*q* SAXS intensity must stem from Li_2S_4 (or other higher-order PS) particles with an electron density larger than the Li_2S electron density. If all generated solid structures were Li_2S with constant electron density, the SAXS intensity changes in **b** should be equal for all *q*.

The required high electron density suggests that higher-order PS solids, such as Li_2S_4 are responsible for the high-*q* intensity shoulder. As shown by DFT calculations[2], higher-order PS solids have a higher mass density and consequently a higher electron density than crystalline Li_2S (Table S2). Amorphous Li_2S has a lower density than crystalline Li_2S and can be ruled out to be responsible for the high q intensity shoulder.

A similar high-*q* intensity shoulder is present in the Li_2S_2 and Li_2S_3 PS solids formed via chemical routes (i.e. disproportionation). This further suggests solid Li_2S_4 to be the intensity hump's origin.

Unfortunately, the WAXS data cannot proof the existence of solid Li_2S_4 (or alternative solid PS) particles. Diffraction peaks of crystalline, solid Li_2S_4 are hard to identify, as the particles are small (< 3 nm) and the diffraction peaks broad. The broad peaks may be at similar positions as the Li_2S diffraction peaks and difficult to distinguish from the significant background. Further, any solid Li_2S_4 particles may be amorphous.

Why are the primary Li_2S crystallites with 7 nm in diameter hardly visible with SAXS?

Besides the relatively low electron density contrast between Li_2S and electrolyte, the Li_2S structure likely forms larger aggregate fractal-like structures. Fractal-like structures cause typically a featureless power-law intensity decay, where the primary particle size is not necessarily visible as a distinct intensity hump / peak.

What about carbon – Li_2S / Li_2S_4 cross correlations?

Carbon black – Li_2S / Li_2S_4 cross correlations are most likely responsible for the significant deviation between model fit and experimental data in Fig. 5a. An improved model fit for a glassy carbon electrode with negligible cross correlation in Supplementary Fig. 5a indicates this (the glassy carbon beads are much larger than the Li_2S /Li_2S_4 deposits).

Supplementary Note 2 | The PGRF model input parameters

Given the possible systematic errors in the SAXS data interpretation, it is feasible to reproduce the experimental SAXS intensities during discharge and charge by varying the PGRF SAXS model input parameters within physically reasonable constraints according to the state of charge. The model fit in Fig. 5a for the Li_2S / Li_2S_4 structure provides the model input parameters after full discharge and serves as a starting point for the input parameter variation shown in Supplementary Fig. 10.

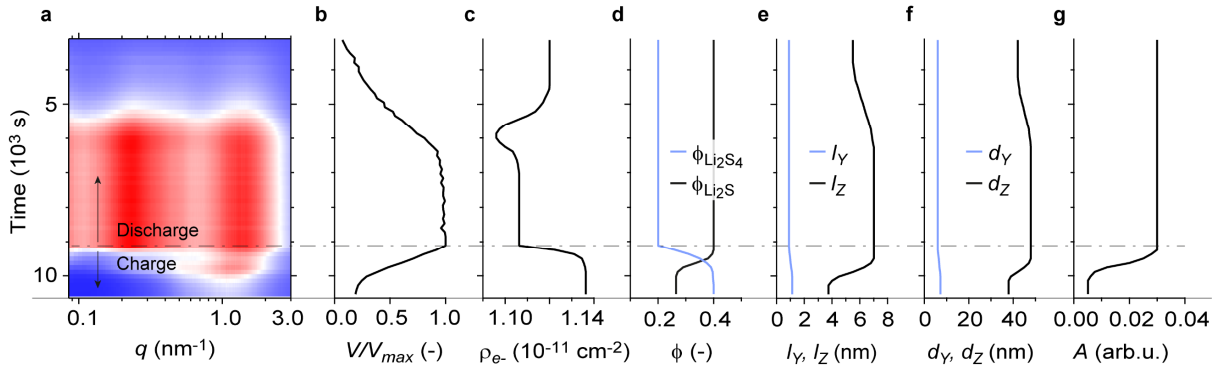

Supplementary Figure 10: Plurigaussian random field model input parameters. **a**, Modelled relative SAXS intensity change during potentiostatic discharge/charge (equivalent data in Fig. 5e). **b**, Relative volume change of the Li_2S / Li_2S_4 nanostructure as a function of time. The amount is proportional to the Li_2S (111) diffraction peak intensity quantified by the Lorentzian model fit in Fig. 2b. **c**, Mean electrolyte electron (scattering length) density as a function of time (given in units of cm^{-2}, ρ_{e^-} corresponds to the electron density times the classical electron radius, 2.82×10^{-13} cm). A subtle q-independent intensity maximum at 5000 – 6000 s (see Fig. 2c-d, Fig. 5d) indicates a minimum in the electrolyte electron density, due to a depletion of dissolved polysulfides at maximum current or maximum Li_2S formation rate. During charge at 2.4 V vs. Li/Li^+, the electrolyte electron density increases due to the higher concentration of heavy $TFSI^-$ anions[6] compensating the more positive electrode potential. Assumed scattering length densities of catholyte, Li_2S, Li_2S_4, and carbon are given in Table S2. **d**, Li_2S_4 and Li_2S volume fractions as a function of time. Apart from charge, the Li_2S volume fraction is assumed to be twice the Li_2S_4 volume fractions. **e**, Correlation parameters l_Y and l_Z of the two Gaussian random fields $Y(\mathbf{x})$ and $Z(\mathbf{x})$. The slight increase of l_Y during charge indicates the slight growth of Li_2S_4 particles at initial stages of charge. The increase of l_z during discharge indicates the growth of the larger Li_2S aggregates; the decrease of l_Y the dissolution of Li_2S aggregates. **f**, Correlation parameters d_Y and d_Z of the two Gaussian random fields $Y(\mathbf{x})$ and $Z(\mathbf{x})$. **g**, Factor A (see Equation 2) as a function of time. The drop during charge accounts for the dissolution of larger Li_2S aggregates. All other input parameters are kept constant (Table S1).

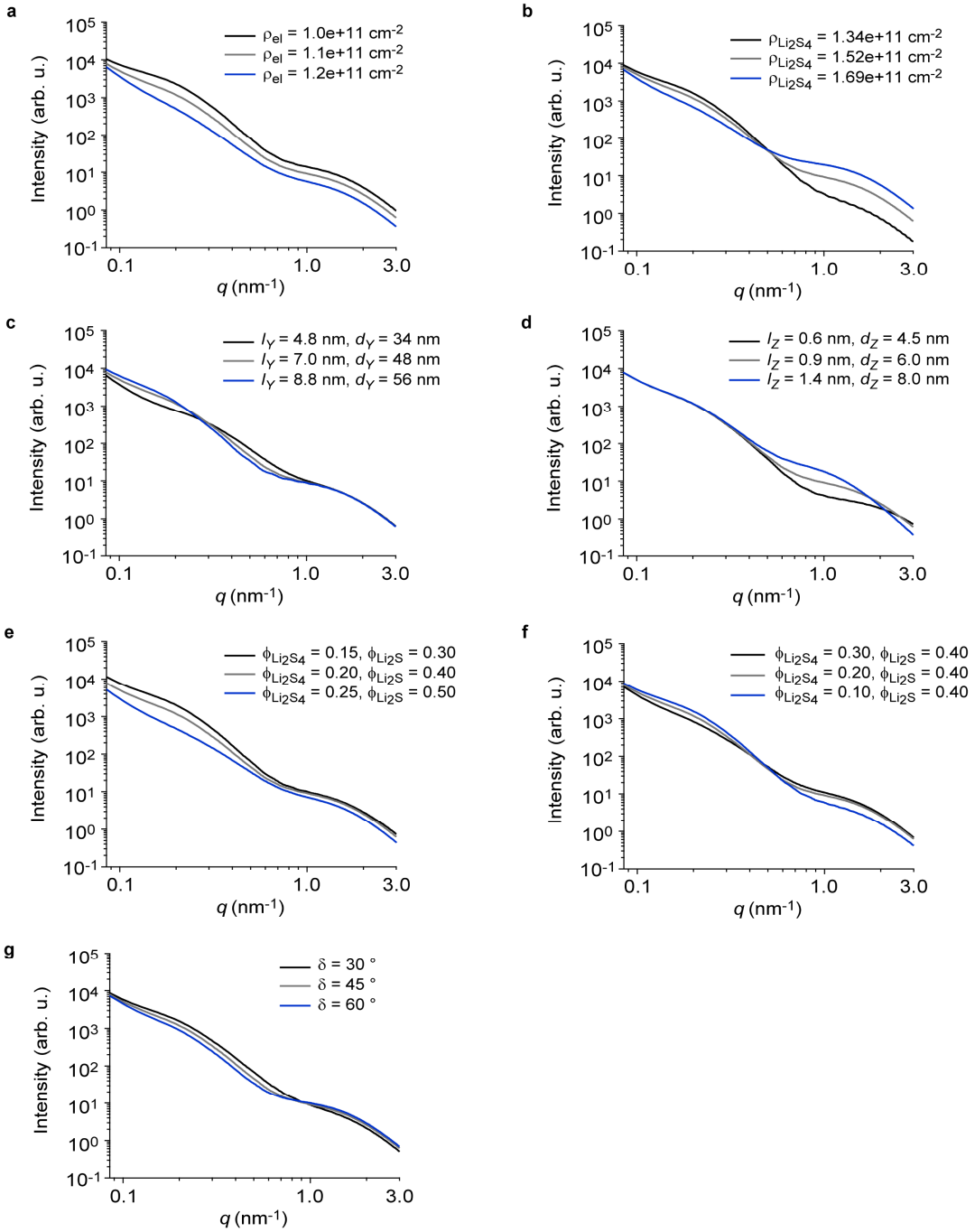

Supplementary Figure 11: Impact of parameter variation on the PGRF model SAXS intensities. The basic parameter configuration corresponds to the values given in Table S2, first column and the model fit shown in Fig. 5a. **a**, SAXS intensity versus scattering vector length *q* for different electrolyte electron (scattering length) densities, while leaving all other parameters constant. **b**, SAXS intensity versus scattering vector length q for different Li_2S_4 electron (scattering length) densities, while leaving all other parameters constant. This shows that the high-q intensity shoulder (Fig. 2, Fig, 5) must stem from particles with an electron density higher than the Li_2S electron density of 1.34×10^{11} cm^{-2}. This points at solid, higher order polysulfides (such as Li_2S_4) with higher mass density compared to solid Li_2S. **c**, SAXS intensity versus scattering vector length *q* for different correlation parameters of the Gaussian random field $Y(\mathbf{x})$, while leaving all other parameters constant. Changes concern mainly the low-q intensity shoulder of Li_2S aggregates. **d**, SAXS intensity versus scattering vector length *q* for different correlation parameters of the Gaussian random field $Z(\mathbf{x})$, while leaving all other parameters constant. Changes concern mainly the high-q intensity shoulder of Li_2S_4 particles. **e-f**, SAXS intensity versus scattering vector length *q* for different Li_2S and Li_2S_4 volume fractions, while leaving all other parameters constant. **g**, SAXS intensity versus scattering vector length *q* for different parameters β, while leaving all other parameters constant. δ determines whether the Li_2S_4 particles grow preferably on top of the Li_2S surface (low δ) or without any cross correlation to the Li_2S structure, i.e. towards the center of the Li_2S cavities (high δ).

Supplementary References

1 Ye, H., Li, M., Liu, T., Li, Y. & Lu, J. Activating Li2S as the Lithium-Containing Cathode in Lithium–Sulfur Batteries. *ACS Energy Letters* **5**, 2234-2245, (2020).

2 Xiao, J. *et al.* Elaboration of Aggregated Polysulfide Phases: From Molecules to Large Clusters and Solid Phases. *Nano Letters* **19**, 7487-7493, (2019).

3 Bahadur, J. *et al.* SANS investigations of CO2 adsorption in microporous carbon. *Carbon* **95**, 535-544, (2015).

4 Prehal, C. *et al.* A carbon nanopore model to quantify structure and kinetics of ion electrosorption with in situ small angle X-ray scattering. *Phys. Chem. Chem. Phys.* **19**, 15549, (2017).

5 Prehal, C. *et al.* In situ small angle X-ray scattering reveals solution phase discharge of Li-O2 batteries with weakly solvating electrolytes. *PNAS* **118**, e2021893118, (2021).

6 Prehal, C. *et al.* Quantification of ion confinement and desolvation in nanoporous carbon supercapacitors with modelling and in situ X-ray scattering. *Nature Energy* **2**, 16215, (2017).